

## A Composite Sb-doped SnO<sub>2</sub> Electrode Based on the TiO<sub>2</sub> Nanotubes Prepared by Hydrothermal Synthesis

Hao Xu<sup>1,2</sup>, Qian Zhang<sup>1</sup>, Wei Yan<sup>1,3\*</sup>, W Chu<sup>2</sup>

<sup>1</sup> Department of Environmental Science and Technology, Xi'an Jiaotong University, Xi'an 710049, China

<sup>2</sup> Department of Civil and Structural Engineering, The Hong Kong Polytechnic University, Hung Hom, Kowloon, Hong Kong

<sup>3</sup> Suzhou Academy, Xi'an Jiaotong University, Suzhou 215012, China

\*E-mail: [yanwei@mail.xjtu.edu.cn](mailto:yanwei@mail.xjtu.edu.cn)

Received: 10 October 2011 / Accepted: 5 November 2011 / Published: 1 December 2011

---

A hydrothermal synthesis approach was adopted to embed Sb-doped SnO<sub>2</sub> into TiO<sub>2</sub> nanotubes to form a three dimensional electrode(TiO<sub>2</sub>-NTs/SnO<sub>2</sub>-Sb), and it was compared with the conventionally fabricated Ti/SnO<sub>2</sub>-Sb<sub>2</sub>O<sub>5</sub> electrode(Sb-doped SnO<sub>2</sub> coated Ti sheet) in terms of surface morphology, crystal structure, photoelectrochemical properties and organic degradation performances. It was clearly observed from SEM images that the TiO<sub>2</sub>-NTs/SnO<sub>2</sub>-Sb electrode had a compact surface and the Sb-doped SnO<sub>2</sub> oxide was embedded successfully into the TiO<sub>2</sub> nanotubes. The loading amount of Sb-SnO<sub>2</sub> in the TiO<sub>2</sub> nanotube electrode was therefore increased compared with that in the Ti/SnO<sub>2</sub>-Sb electrode, which is beneficial for the electrochemical performance. The hydrothermally synthesized electrode has much better and larger SnO<sub>2</sub> crystals than that prepared by the traditional dip-coating method according to the Scherrer's equation derived from the XRD analysis. Besides, the durability of the TiO<sub>2</sub>-NTs/SnO<sub>2</sub>-Sb electrode was tested to be 116 hours, which was much longer than that of the Ti/SnO<sub>2</sub>-Sb electrode (1.6 hours), suggesting a long service lifetime electrode was achieved through the hydrothermal method. A higher oxygen evolution potential leading to a preferred degradation of methyl orange in an electro-catalytic process was observed by using the hydrothermally-prepared electrode than that of Ti/SnO<sub>2</sub>-Sb electrode. The TiO<sub>2</sub>-NTs/SnO<sub>2</sub>-Sb electrode has a superior ability in coupling the advantages of photocatalysis and electrocatalysis, which was evidenced by the linear sweep voltammetry and the chronoamperometry tests. It was interesting to note that an irradiation from Xenon lamp originally has no effect on the probe dye's removal. However, as the same irradiation was introduced to the electrocatalysis process using the TiO<sub>2</sub>-NTs/SnO<sub>2</sub>-Sb electrode, the removal efficiency of the probe significantly increased from 15.7% to 26.9% in 2 hours, due to a synergetic effect.

---

**Keywords:** TiO<sub>2</sub> nanotubes; hydrothermal synthesis; Sb-doped SnO<sub>2</sub>; electrocatalysis; photoelectrocatalysis

## 1. INTRODUCTION

In the past decade, the electrochemical oxidation technology has gained worldwide attention due to its outstanding performance for the pollutants' elimination [1-3]. The photochemical oxidation, as another leading approach of the advanced oxidation technologies, also attracts significant interests because of its high oxidative-ability in the degradation of non-biodegradable organic pollutants [4, 5]. Thus, the combination of these two technologies has become a recent issue in water industry. With the assistance of externally applied electric field, photo-generated electrons are able to migrate to the counter electrode along the potential gradient resulting in an effective separation of the charge carriers. This facilitates the oxidative capacity of photo-generated holes and further enhances the treatment efficiency. Therefore, by loading the photocatalyst on the electrode surface with the assistance of external voltage is considered to be a feasible approach. The crucial part of the efficient electrochemical treatment is associated with the proper selection of anode materials. Materials with high corrosion resistances, physical and chemical stability under high positive potentials are therefore extensively investigated [6]. Antimony doped SnO<sub>2</sub>, with its excellent electrocatalytic performance, was found to be the most suitable material for the anode in the degradation of organic contaminants including phenol, benzoquinone, bisphenol A, and aromatic compounds [7-11]. Nevertheless, the main problem with commercial applications of SnO<sub>2</sub> electrode is the short service lifetime because the binding force between the titanium substrate and the active SnO<sub>2</sub> layer is weak [12-15]. Many efforts have been attempted to solve this problem. For example, introduction of Ir, Ru, Pt and some rare elements [16-20] onto the surface of SnO<sub>2</sub> film could enhance the electrode stability. Titanium dioxide nanotube array, a new type of titanium dioxide nano-material, have drawn extraordinary attention in recent years due to its distinctive morphology and notable performance [21-23]. Owing to the translucent property of SnO<sub>2</sub>, incorporation of SnO<sub>2</sub> with titanium dioxide would not interfere with the light absorption of TiO<sub>2</sub>. Therefore, Zhao *et al.* [14, 15, 24] prepared a novel electrode by implanting tin-antimony oxide sol-gel (with super wetting and spreading properties) into the vertically aligned TiO<sub>2</sub> nanotubes under vacuum conditions. Chen *et.al.* [25] introduced SnO<sub>2</sub>-Sb into the TiO<sub>2</sub>-NTs by the electrodeposition method. This type of electrode has more excellent performance in the stability test than the electrode of Sb<sub>2</sub>O<sub>5</sub> doped SnO<sub>2</sub> on Ti substrate (Ti/SnO<sub>2</sub>-Sb<sub>2</sub>O<sub>5</sub>) prepared by the traditional method.

Currently, there is no difficulty in preparing membrane or film on different substrate surface by hydrothermal synthesis [26, 27]. After the substrate is immersed into the synthesis solution, the membrane/film will be formed by direct crystallization under certain temperature and pressure provided by the hydrothermal environment, which is quite convenient. In this study, the hydrothermal synthesis followed by annealing was proposed to prepare the Sb doped SnO<sub>2</sub> based on the TiO<sub>2</sub> nanotubes (referred to TiO<sub>2</sub>-NTs/SnO<sub>2</sub>-Sb) electrode, where the hydrothermal method was used to overcome the surface tension of TiO<sub>2</sub>-NTs to facilitate the Sb-SnO<sub>2</sub> deposition. The resulted TiO<sub>2</sub>-NTs/SnO<sub>2</sub>-Sb electrode was compared with the Sb doped SnO<sub>2</sub> based on the Ti substrate (Ti/SnO<sub>2</sub>-Sb<sub>2</sub>O<sub>5</sub>) electrode prepared by the dip-coating method via instrument analysis (FESEM, XRD, cyclic voltammetry, chronoamperometry, and accelerated life tests). Methyl orange, a typical azo dye, was

chosen as the degradation probe to determine their catalytic performance in water/wastewater treatment.

## 2. EXPERIMENTAL DETAILS

High purity (99.6% purity) titanium (Ti) foils with thickness of 0.5 mm purchased from BaoTi Co. Ltd. in China were used in this study. All the chemicals used in this work were of analytical grade. The deionized water (18.25 M $\Omega$ ) used was produced by the water purifier (EPET-40TF, EPET Co. Ltd, Nanjing, China).

Prior to the preparation process, Ti foils were mechanically polished with 1000-grit sand papers and rinsed with deionized water. The foils were then immersed into a mixture of acetone and 1 mol·L<sup>-1</sup> NaOH (1:1 v/v) in an ultrasonic cleaner (KQ2200DB, 80W, 40 KHz, Kunshan Ultra Co. Ltd, Jiangsu, China) to remove organic compounds from the surface. It was then followed by an etching process in 10% oxalic acid at 98°C for 2h, and finally washed thoroughly with deionized water.

The electrochemical anodization process was performed in a two-electrode configuration with the Ti foil as the anode and a platinum electrode as the counter electrode. The distance between the cathodic and anodic electrodes was approximately 1.5 cm. The electrolyte (pH=6) consisted of 0.8 wt % NH<sub>4</sub>F (99.5%), 1.6 wt % Na<sub>2</sub>SO<sub>4</sub> (99.5%), and 10 wt % PEG400. The anodization process was carried out at 20V constantly for 3h at room temperature (about 20 °C), accompanied by constant magnetic agitation to reduce the thickness of the double layer at the metal/electrolyte interface and ensure uniform local current density and temperature over the Ti electrode surface[28]. After the anodization process completed, the anodized Ti foil was rinsed with deionized water.

The precursor solution was freshly prepared before use by dissolving 10% SnCl<sub>4</sub>·6H<sub>2</sub>O and 1% SbCl<sub>3</sub> in ethanol and the solution pH was adjusted to 2 by hydrochloric acid. In the dip-coating method, the titanium sheet was brushed with the precursor solution, and subsequently calcined at 450°C in a muffle oven for 15 min. This procedure was repeated for 10 times. Finally, the electrode was annealed at 450°C for an hour to induce crystallization.

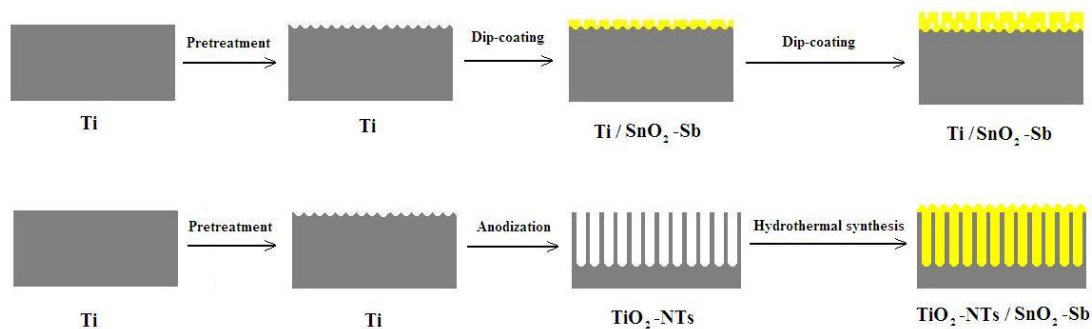


**Figure 1.** Schematic diagram of the dip-coating process on the titanium base and the hydrothermal synthesis on the TiO<sub>2</sub>-NTs base

In the hydrothermal synthesis approach, the anodized TiO<sub>2</sub>-NTs electrode was placed vertically in a Teflon-lined stainless steel reactor, immersed in the precursor solution with the reactor sealed in the end. After crystallation for 24~48 h at 150°C, the solution was drained away and the resulted sample was washed carefully with deionized water. The electrode was air-dried and crystallized by annealing in an air at 450°C for 60 min with a heating rate of 1°C/min in an oven (CMF1100, Hefei Kejin Co. Ltd, China). The schematic diagrams of the two approaches are shown in Figure 1.

The morphology of the electrodes was characterized using a field emission scanning electron microscope (FESEM, JEOL, and JSM-6700F). The crystal structure of the electrodes after annealing treatment was identified by a X'pert PRO MRD diffractometer with Cu-K<sub>α</sub> radiation (0.15416 nm). The electrochemical characteristics of the two electrodes were measured separately in a three-electrode system with the prepared electrode served as the working electrode, Pt foil as the counter electrode, and Ag/AgCl/saturated KCl electrode as the reference electrode, respectively. The electrochemical measurements were conducted on the electrochemical analysis system (LK3200A, Lanlike, China). The measurements include the cyclic voltammetry test, the linear sweep voltammetry at a scan speed of 20 mV·s<sup>-1</sup> in 20 g·L<sup>-1</sup> Na<sub>2</sub>SO<sub>4</sub> solution at room temperature and the accelerated lifetime test at a current density of 100mA·cm<sup>-2</sup> in 1.0 mol·L<sup>-1</sup> Na<sub>2</sub>SO<sub>4</sub> solution at 30~35°C.

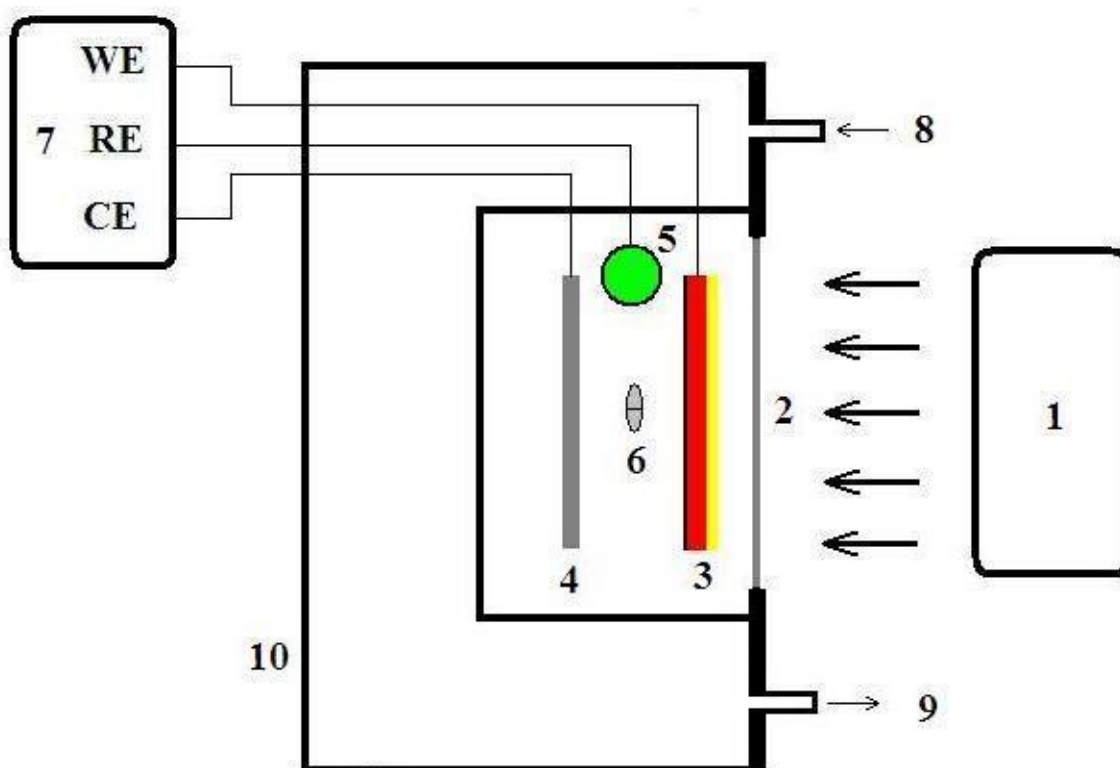


**Figure 2.** Schematic diagram of the electro/photo-electro catalysis experimental system, 1: light source; 2: quartz glass; 3: the prepared electrode; 4: Pt electrode; 5: Ag/AgCl reference electrode; 6: stirrer; 7: electrochemical analysis system; 8: cooling water in; 9: cooling water out; 10: plexiglass reactor

All the organic pollutant degradation tests were conducted in the system as shown in Figure 2. In the degradation process, as 250 ml methyl orange wastewater ( $200 \text{ mg}\cdot\text{L}^{-1}$ ) was added into the plexiglass reactor, the stirring, the control system, and the cooling system were turned on simultaneously. For the photoelectrocatalysis process, the Xenon lamp (CHF-XM-500W, Trusttech Co Ltd., Beijing, China) was powered on before the reaction began to ensure a stabilized light source. The electrocatalysis and the photoelectrocatalysis processes were both carried out under a constant current condition ( $10 \text{ mA}\cdot\text{cm}^{-2}$ ) for 2 hours, separately. During the treatment process, the wastewater sample was withdrawn every 20 min for the UV-Vis analyses (Agilent 8453).

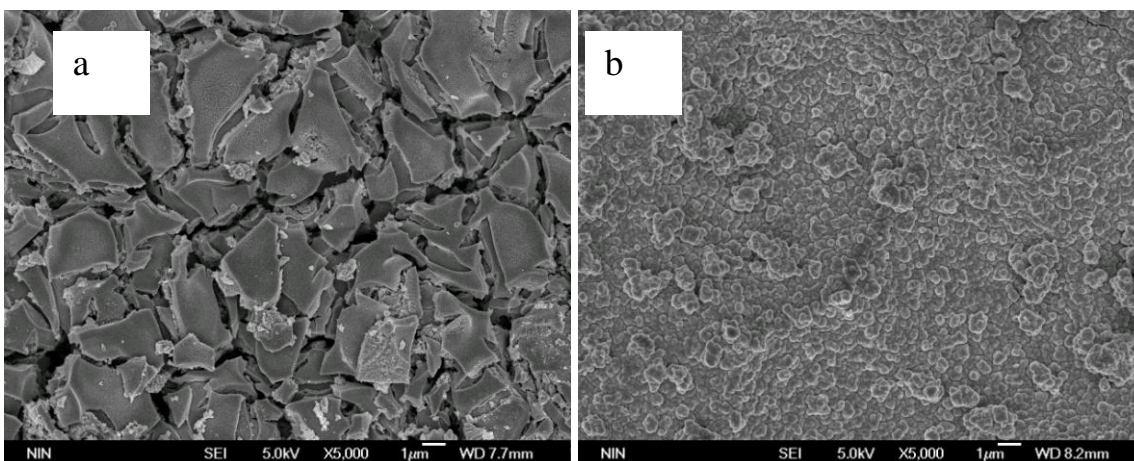
### 3. RESULTS AND DISCUSSION

#### 3.1 Loading amount

As we know, it is an effective way to enhance electrodes' electrochemical ability by increasing the electrocatalyst loading [12, 14, 29]. The loading amount of Sb-doped  $\text{SnO}_2$  on the  $\text{Ti}/\text{SnO}_2\text{-Sb}$  electrode was measured to be  $1.10 \text{ mg}\cdot\text{cm}^{-2}$  in this work, which is consistent with earlier reports [11, 14]. In this study, the hydrothermal method was proposed to overcome the surface tension of  $\text{TiO}_2\text{-NTs}$  in order to increase the Sb-doped  $\text{SnO}_2$  loading amount. The loading amount of Sb-doped  $\text{SnO}_2$  in the  $\text{TiO}_2\text{-NTs}/\text{SnO}_2\text{-Sb}$  electrode was increased up to  $2.11 \text{ mg}\cdot\text{cm}^{-2}$ , which is 1.9 times higher than that in the  $\text{Ti}/\text{SnO}_2\text{-Sb}$  electrode. This result was similar with Zhao's work [14]. As shown in Fig.1, it is presumed that due to the large surface area and volume of the  $\text{TiO}_2$  nanotubes, the Sb-doped  $\text{SnO}_2$  is embedded into the nanotubes resulting in the enhancement of the load capacity.

#### 3.2 Surface morphology

Figure 3 shows the FESEM images of the surface morphology of the electrodes fabricated by the two different methods.



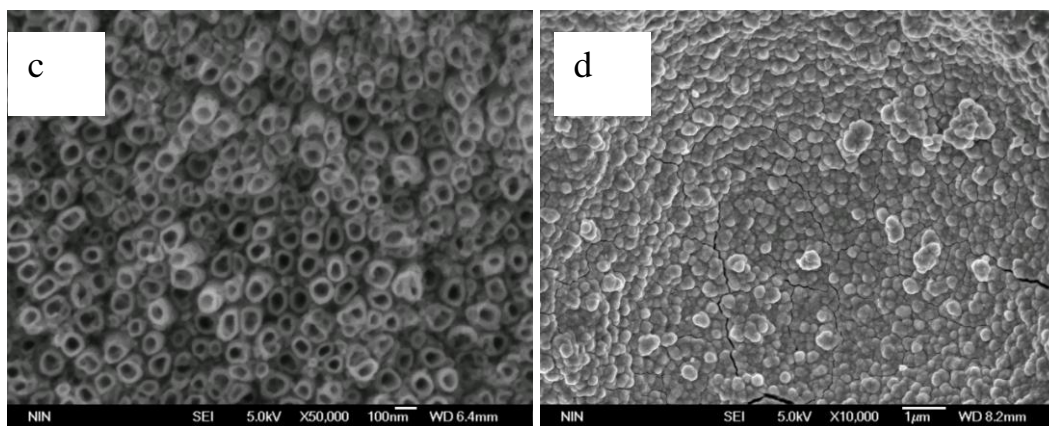


**Figure 3.** FESEM images of the as-prepared samples (a) Ti/SnO<sub>2</sub>-Sb electrode prepared by dip-coating method, (b) and (d) TiO<sub>2</sub>-NTs/SnO<sub>2</sub>-Sb electrode prepared by hydrothermal synthesis method, (c) TiO<sub>2</sub>-NTs prepared by the electrochemical anodization

It can be observed from Figure 3(a) that the Ti/SnO<sub>2</sub>-Sb electrode prepared by the dip-coating method exhibits a typical cracked-mud structure [30], which facilitates the electrolyte's diffusion into the Ti substrate, accelerates the formation of TiO<sub>2</sub> with poor conductivity and the subsequent peeling off of Sb-doped SnO<sub>2</sub> film. On the contrary, the surface of the TiO<sub>2</sub>-NTs/SnO<sub>2</sub>-Sb electrode (see Figure 3(b)) is much smoother and more compact than the Ti/SnO<sub>2</sub>-Sb. Furthermore, the substrate fully covered by the Sb-doped SnO<sub>2</sub> film with no cracked-mud structure can be found. This can be further confirmed by the higher magnification image in-Fig. 3(d). The superior surface morphology in Fig. 3(b) may contribute to a longer accelerated life span of the TiO<sub>2</sub>-NTs/SnO<sub>2</sub>-Sb electrode than that of the Ti/SnO<sub>2</sub>-Sb electrode. The image of well-aligned and uniform TiO<sub>2</sub> nanotubes growing on the Ti substrate fabricated in this work is displayed in Fig. 3(c). It is clearly noted that the openings of the nanotubes are in circular and/or oval shapes, and the average diameter of these nanotubes ranges from 70 to 90 nm with wall thickness of 10–20 nm. By comparing Figure 3(c) and 3(d), it is interesting to note that the Sb-doped SnO<sub>2</sub> oxide forms a similar structure corresponding to the opening shape of the nanotubes, suggesting the possibility of Sb-doped SnO<sub>2</sub> embedded into the TiO<sub>2</sub> nanotubes.

### 3.3 XRD analysis

Figure 4 compares the XRD patterns of the TiO<sub>2</sub>-NTs/SnO<sub>2</sub>-Sb and the Ti/SnO<sub>2</sub>-Sb electrodes prepared by distinct methods mentioned above. It can be noticed that TiO<sub>2</sub> with rutile and anatase phases corresponding to (110), (002) and (101), (004) peaks are found in the TiO<sub>2</sub>-NTs as shown in curve 2. In the XRD pattern of Ti/SnO<sub>2</sub>-Sb electrode (curve 1), the peaks at 26.6° (110), 34° (101), and 51.9° (211) are the characteristic peaks of the rutile SnO<sub>2</sub>, which indicates the crystalline structure of SnO<sub>2</sub> coated on the surface of the electrode [24, 31]. However, the corresponding peaks assigned to TiO<sub>2</sub> are overlapped by the strong SnO<sub>2</sub> peaks. Besides, no additional peaks corresponding to antimony oxides are detected. Compared with the Ti/SnO<sub>2</sub>-Sb electrode synthesized by the traditional method, the half-widths of the reflection peaks of SnO<sub>2</sub> of the novel electrode are reduced, which

suggests better and larger crystals of  $\text{SnO}_2$  are formed in the newly fabricated electrode. The reflection intensity of the Ti peaks of the  $\text{TiO}_2\text{-NTs/SnO}_2\text{-Sb}$  electrode is lower than that of the  $\text{Ti/SnO}_2\text{-Sb}$  electrode, which suggests the former has a denser surface than the latter.

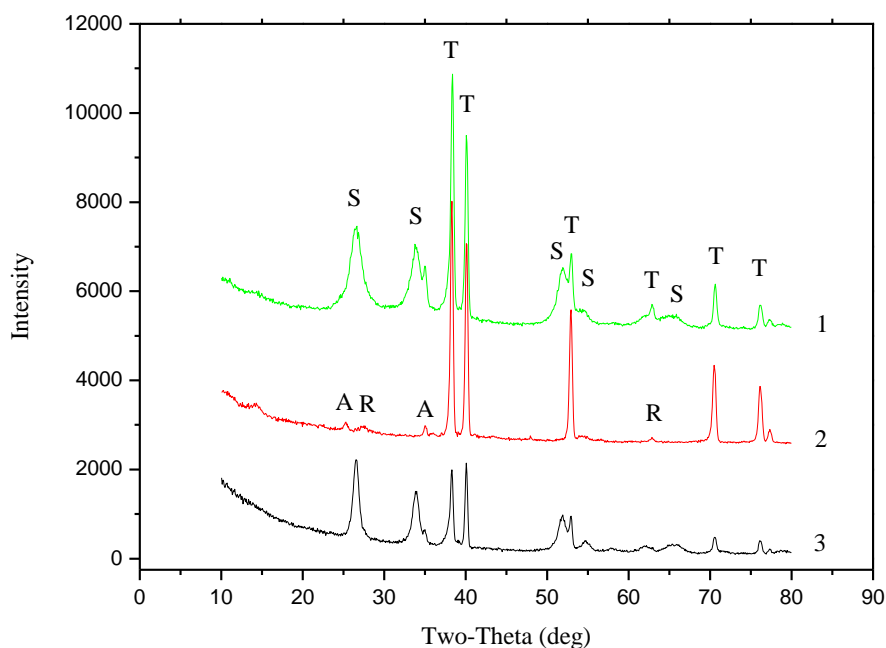


**Figure 4.** XRD patterns of the as-prepared samples 1  $\text{Ti/SnO}_2\text{-Sb}$  electrode; 2  $\text{TiO}_2\text{-NTs}$  foil; 3  $\text{TiO}_2\text{-NTs/SnO}_2\text{-Sb}$  electrode; S represents  $\text{SnO}_2$ ; T represents titanium; R represents  $\text{TiO}_2$  rutile; A represents  $\text{TiO}_2$  anatase

According to the Scherrer formula [24], the average crystal size of Sb-doped  $\text{SnO}_2$  particles measured by XRD was calculated to be about 28 and 33 nm for the  $\text{Ti/SnO}_2\text{-Sb}$  and the  $\text{TiO}_2\text{-NTs/SnO}_2\text{-Sb}$  electrodes, respectively.

### 3.4 Accelerated life test

Common Sb-doped  $\text{SnO}_2$  electrodes are often restricted in application of wastewater treatment primarily due to its relatively short service life. Thus the electrochemical stability of the two electrodes fabricated in this work was compared through the accelerated life test. Figure 5 depicts the potential variation with time of the two electrodes in the tests, where significant differences between the two curves were observed. In Figure 5(a), the potential of the  $\text{Ti/SnO}_2\text{-Sb}$  electrode jumped sharply to 9.5 V within 10 min, then slowly approached to 10 V (vs Ag/AgCl) in 1.6 h. This may be attributed to the formation of the  $\text{TiO}_2$  insulation layer between the Sb-doped  $\text{SnO}_2$  layer and the titanium substrate. On the contrary, the potential of the  $\text{TiO}_2\text{-NTs/SnO}_2\text{-Sb}$  electrode remained steady at around 2.7-3.2V for the first 80 hours, then it increased to 10 V (vs Ag/AgCl) after 116 hours of operation, as shown in Fig.5(b). This suggests that the Sb-doped  $\text{SnO}_2$  layer is consumed uniformly throughout the process.

As evidenced by the SEM images of these two electrodes, the  $\text{TiO}_2\text{-NTs/SnO}_2\text{-Sb}$  electrode has a continuous and compact surface layer without any obvious cracks on the surface (Figures 3(b) and 3(d)), suggesting the electrolyte is difficult to diffuse into the titanium substrate and the stability of the electrode is ensured.

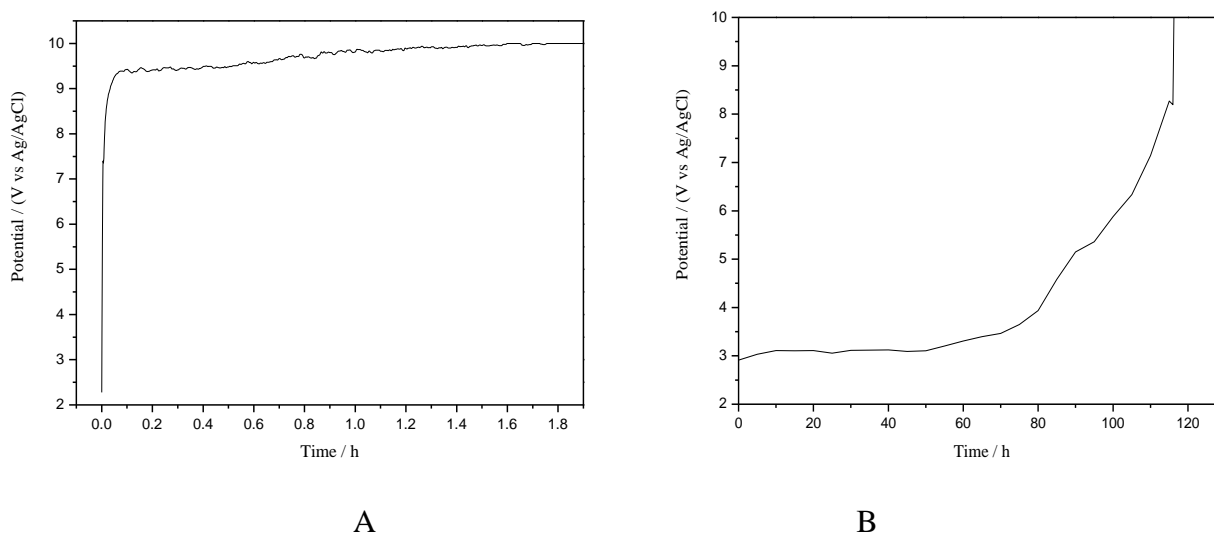


**Figure 5.** Potential variation with time in accelerated life tests performed in  $1 \text{ mol}\cdot\text{L}^{-1} \text{Na}_2\text{SO}_4$  solution under  $100 \text{ mA}\cdot\text{cm}^{-2}$  for (a)  $\text{Ti/SnO}_2\text{-Sb}$  electrode and (b)  $\text{TiO}_2\text{-NTs/SnO}_2\text{-Sb}$  electrode

As the current density and electrolyte are kept constant, the potential increase is only resulted from the rise of the electrode resistance, which justifies the quality of the electrode itself. By using 10 V as a standard value to define the deactivation of the electrode, the service life of the  $\text{TiO}_2\text{-NTs/SnO}_2\text{-Sb}$  electrode is 116 h comparing to that of  $\text{Ti/SnO}_2\text{-Sb}$  electrode for only 1.6h. This result is in consistent with the previous studies [30].

### 3.5 Cyclic voltammetry

Figure 6 shows the cyclic voltammetry curves of the two electrodes in the  $20 \text{ g}\cdot\text{L}^{-1} \text{Na}_2\text{SO}_4$  solution at a scan rate of  $20 \text{ mV}\cdot\text{s}^{-1}$ , where no reaction peaks were observed except the oxygen evolution peak. In general, the oxygen evolution potential is a crucial factor influencing the anode activity. A higher evolution potential can effectively decrease the rate of oxygen evolution, increase the degradation efficiency of organics via oxidation in wastewater treatment, and reduce the energy consumption [27]. In Fig. 6, the  $\text{TiO}_2\text{-NTs/SnO}_2\text{-Sb}$  electrode shows a slightly higher oxygen evolution potential of 1.78 V comparing to 1.73 V for the  $\text{Ti/SnO}_2\text{-Sb}$  electrode at  $1.0 \text{ mA}\cdot\text{cm}^{-2}$ . This can be attributed to the XRD analysis that the average crystal size of Sb-doped  $\text{SnO}_2$  particles on the two electrodes was different. From previous research [14], the mechanism of the  $\text{SnO}_2$  electrode in oxidizing pollutants is initiated by splitting water into hydroxyl radicals and subsequent adsorption of hydroxyl radicals on the electrode's surface. Then, the hydroxyl radicals can oxidize pollutants (R)

into intermediates and eventually produce  $\text{CO}_2$  and  $\text{H}_2\text{O}$  if the level of radical concentration is high enough. However, the collision and combination of hydroxyl radicals may generate  $\text{O}_2$  as byproduct to compete with the organic degradation reaction, as shown in Eqs. 1 and 3.

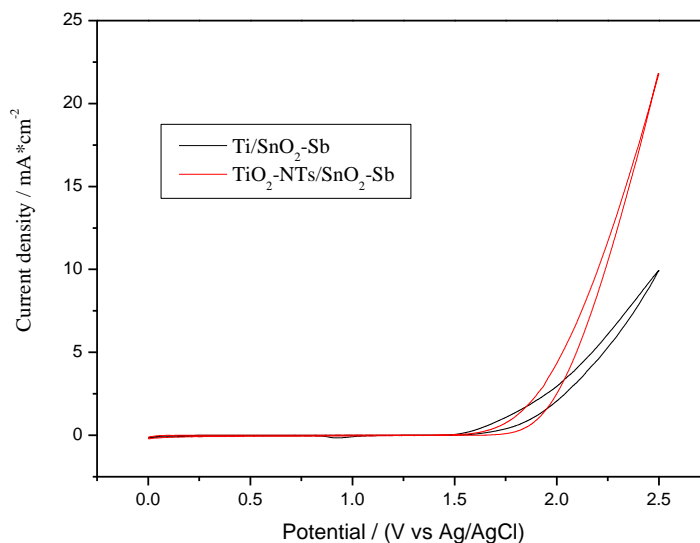


**Figure 6.** Cyclic voltammety curve of various  $\text{SnO}_2$  electrodes in  $20 \text{ g}\cdot\text{L}^{-1}$   $\text{Na}_2\text{SO}_4$  solution at a scan rate of  $20 \text{ mV}\cdot\text{s}^{-1}$

The  $\text{TiO}_2\text{-NTs/SnO}_2\text{-Sb}$  electrode has a much larger crystal size, which hinders the recombination rate of adsorbed hydroxyl radicals (to produce  $\text{O}_2$ ) in a completely mixed reactor. This is likely to be the reason causing a higher oxygen evolution potential for the  $\text{TiO}_2\text{-NTs/SnO}_2\text{-Sb}$  electrode.

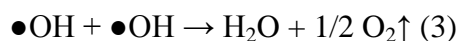
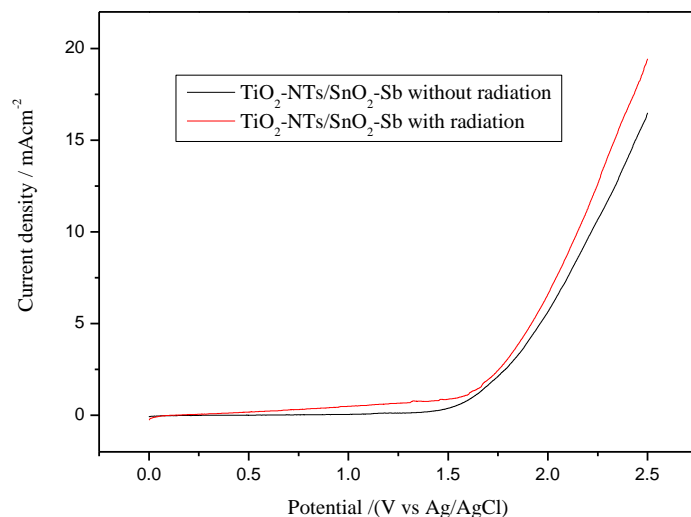
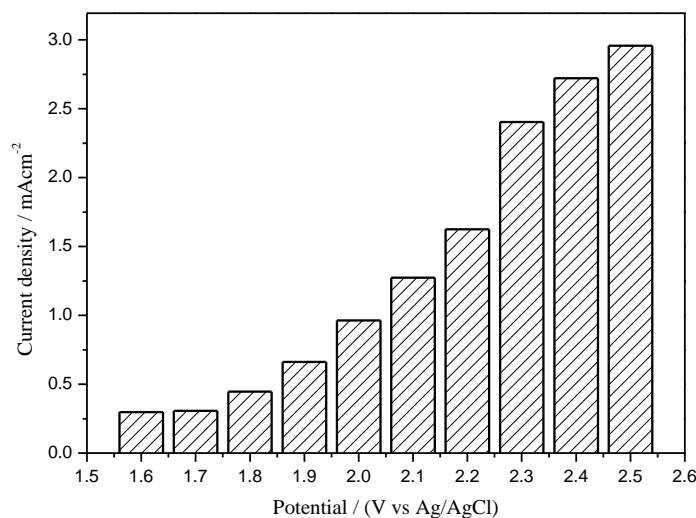


Figure 7a shows the cyclic voltammety curves of the hydrothermally prepared  $\text{TiO}_2\text{-NTs/SnO}_2\text{-Sb}$  electrode with and without light irradiation. It can be observed that under the identical potential the current density with light is much higher than that without light. Specifically, at the sweeping potential of  $2.0 \text{ V}$ , the current density was  $5.64 \text{ mA}\cdot\text{cm}^{-2}$  in the dark, while that was  $6.60 \text{ mA}\cdot\text{cm}^{-2}$  under illumination, with a difference of  $0.96 \text{ mA}\cdot\text{cm}^{-2}$ . The current density difference can be explained by the photo-generated carriers transport imposed by the electric force separation, apart from the current resulting from the oxygen evolution process. It indicates that the  $\text{TiO}_2\text{-NTs/SnO}_2\text{-Sb}$  electrode possesses the light responsive property and can be applied as photoelectrode.



A



B

**Figure 7.** Linear sweep voltammetry of TiO<sub>2</sub>-NTs/SnO<sub>2</sub>-Sb electrode with and without radiation in 20 g·L<sup>-1</sup> Na<sub>2</sub>SO<sub>4</sub> solution at a scan rate of 20 mV·s<sup>-1</sup> (a) LSV curve; (b) the curve of the current density difference versus applied potential

To further investigate the effect of light illumination on the photoelectrochemical performance, the current density difference with and without light versus externally applied potential was plotted shown in Figure 7b. From the bar chart we can tell that with the increase in sweeping potential the current density difference also gradually increased. For instance, when the applied potential was at 1.7V、2.0V and 2.4V, the corresponding current difference was 0.31 mA·cm<sup>-2</sup>、0.96 mA·cm<sup>-2</sup> and 2.72 mA·cm<sup>-2</sup>, respectively. This suggests that with enhancement in electric field intensity, the separation degree of photo-generated carriers was significantly increased, leading to an obvious increase in current density in the external circuit.

Figure 8 is the schematic diagram of the photoelectrocatalytic process. When  $\text{TiO}_2$  is irradiated with light, electrons in the valence band absorb the energy and excite to the conduction band, becoming the photo-generated electrons.

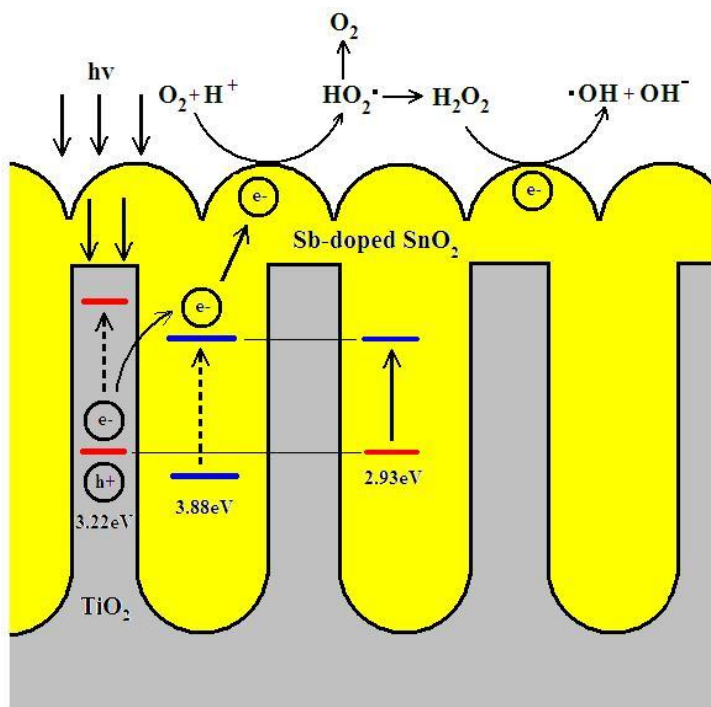


**Figure 8.** Schematic diagram of the photoelectrocatalytic process

Because the surface of the  $\text{TiO}_2$  nanotubes was covered with  $\text{SnO}_2$ , only the photo-generated electrons can diffuse to the electrode surface to react with  $\text{O}_2$  to form  $\text{HO}_2^\bullet$  and subsequently the  $^\bullet\text{OH}$ , as reported previously [15]. By assisting the photocatalytic process with electric field, the photo-generated electrons can promptly migrate to the counter electrode, which further reduces the chance of recombination with photo-generated holes. The synergic effect is potentially useful in degrading organic pollutants that are recalcitrant to electrochemical or heterogeneous photocatalytic treatments [6].

### 3.6 Chronoamperometry

The chronoamperometry method was used to test the photoelectrocatalytic characteristics of the  $\text{TiO}_2$ -NTs/ $\text{SnO}_2$ -Sb electrode. As shown in Figure 9, there was no current in the first 400 s for the non-irradiation electrode at 0.5 V. When the  $E_{\text{anode}}$  increased to 1.5 V, which was lower than the oxygen evolution potential of the  $\text{TiO}_2$ -NTs/ $\text{SnO}_2$ -Sb electrode, a small enhancement of  $0.09 \text{ mA}\cdot\text{cm}^{-2}$  in current density was observed. When light source was introduced to the process, however, a significant difference was observed. In the first stage ( $E_{\text{anode}} = 0.5 \text{ V}$ ), the background current density was  $0.045 \text{ mA}\cdot\text{cm}^{-2}$ , which was a little higher than the non-irradiation system. When the  $E_{\text{anode}}$  increased to 1.5 V,

the current density showed a steep increment to  $0.55 \text{ mA}\cdot\text{cm}^{-2}$ , which was almost 6.1 times higher than that in the non-irradiation test. The result reveals that the  $\text{TiO}_2\text{-NTs/SnO}_2\text{-Sb}$  electrode has a superior ability to combine the advantages of the photochemical and electrochemical processes.

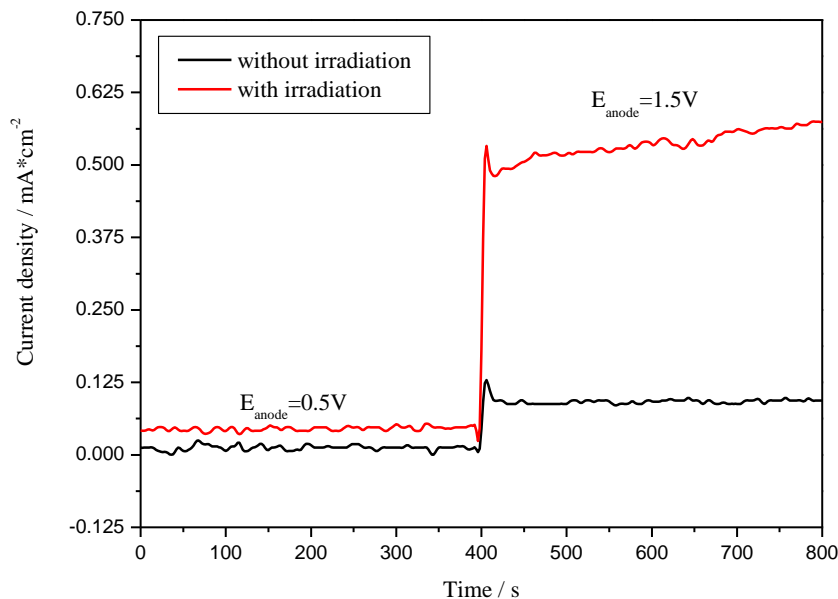


**Figure 9.** Chronoamperometry spectrum of the  $\text{TiO}_2\text{-NTs/SnO}_2\text{-Sb}$  electrode with and without radiation in  $20 \text{ g}\cdot\text{L}^{-1} \text{Na}_2\text{SO}_4$  solution

### 3.7 Electrocatalysis and photo-electrocatalysis

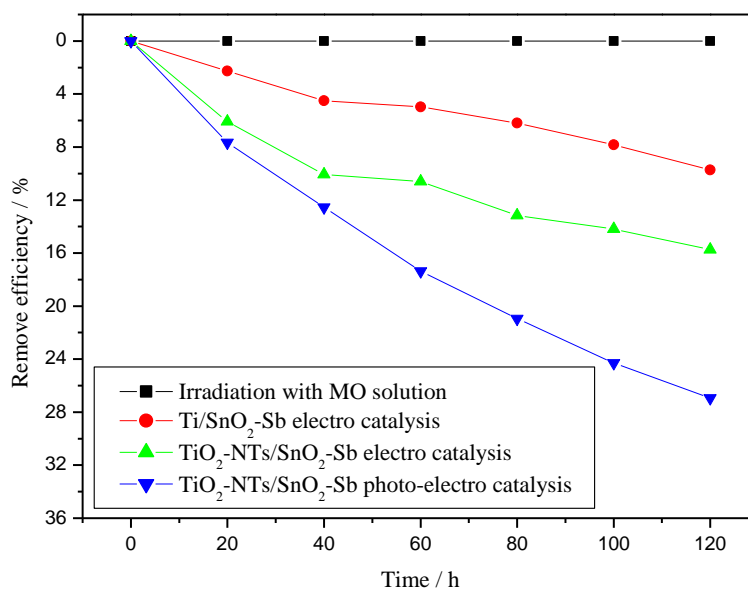


**Figure 10.** Degradation results for various kinds situation in solution consistent of  $50 \text{ mg}\cdot\text{L}^{-1}$  methyl orange and  $20 \text{ g}\cdot\text{L}^{-1} \text{Na}_2\text{SO}_4$

Figure 10 compares the degradation results of methyl orange (MO) solution in different conditions, including irradiation alone, electrocatalysis with the Ti/SnO<sub>2</sub>-Sb electrode, the TiO<sub>2</sub>-NTs/SnO<sub>2</sub>-Sb electrode, and photoelectrocatalysis with the TiO<sub>2</sub>-NTs/SnO<sub>2</sub>-Sb electrode. It is evident that the TiO<sub>2</sub>-NTs/SnO<sub>2</sub>-Sb electrode has a better performance in the electrocatalytic degradation of MO than the Ti/SnO<sub>2</sub>-Sb electrode does, with removal efficiency of 15.7% and 9.7% after electrocatalysis for 2 hours, respectively. This can be explained by the high oxygen evolution potential of the TiO<sub>2</sub>-NTs/SnO<sub>2</sub>-Sb electrode as discussed before. In addition, the synergetic effect in combining photocatalysis and electrocatalysis processes was also observed for the TiO<sub>2</sub>-NTs/SnO<sub>2</sub>-Sb electrode. From the curves, the decay of MO by the sole irradiation was insignificant, while 15.7% of MO was removed by the use of TiO<sub>2</sub>-NTs/SnO<sub>2</sub>-Sb electrode in electrocatalysis process. However, the removal efficiency further increased to 26.9% in 2 hours in the presence of light illumination (i.e. photoelectrocatalysis process). The reason for the improvement in the removal efficiency is mainly due to the electric bias potential which promotes the prompt separation of the photo-generated electrons and holes, thus minimize the fast recombination and a better removal efficiency of MO is obtained.

#### 4. CONCLUSIONS

In this work, a three dimensional TiO<sub>2</sub>-NTs/SnO<sub>2</sub>-Sb electrode was prepared by using the hydrothermal synthesis. The loading amount of Sb-doped SnO<sub>2</sub> in the TiO<sub>2</sub>-NTs/SnO<sub>2</sub>-Sb electrode is significantly lifted, compared with the Ti/SnO<sub>2</sub>-Sb electrode. According to the SEM images, the TiO<sub>2</sub>-NTs/SnO<sub>2</sub>-Sb electrode has a more compact surface and the Sb-doped SnO<sub>2</sub> oxide is successfully embedded into the TiO<sub>2</sub> nanotubes. The TiO<sub>2</sub>-NTs/SnO<sub>2</sub>-Sb electrode has a better and larger crystal of SnO<sub>2</sub> compared with the Ti/SnO<sub>2</sub>-Sb electrode prepared by the traditional method, which is thought to be mainly responsible for the higher photo-electrocatalytic performance. The service life of the TiO<sub>2</sub>-NTs/SnO<sub>2</sub>-Sb electrode is measured to be 116 hours, much longer than the Ti/SnO<sub>2</sub>-Sb electrode. The TiO<sub>2</sub>-NTs/SnO<sub>2</sub>-Sb electrode also has a higher oxygen evolution potential of 1.78 V at 1.0 mA·cm<sup>-2</sup> than the Ti/SnO<sub>2</sub>-Sb electrode, which leads to a better removal efficiency in the electrocatalytic degradation of methyl orange. The TiO<sub>2</sub>-NTs/SnO<sub>2</sub>-Sb electrode has the superior ability to couple the merits of the photochemical and electrochemical process, which is verified by the cyclic voltammetry and the chronoamperometry tests under conditions with or without irradiation. The decay of MO by the sole irradiation was found to be negligible and 15.7% of MO was removed by the use of TiO<sub>2</sub>-NTs/SnO<sub>2</sub>-Sb electrode in electro catalysis process. In photo-electrocatalysis process, however, the removal efficiency further increased to 26.9% in 2 hours indicating the existence of a synergetic effect.

#### ACKNOWLEDGMENTS

The authors gratefully acknowledge the financial support from the Ph. D. Programs Foundation of Ministry of Education of China (20090201110005), Natural Science Foundation of Jiangsu Province, China (SBK201022919) and the Hong Kong Polytechnic University (GU-784).

## References

1. M. Panizza, G. Cerisola, *J. Hazard. Mater.* 153 (2008) 8
2. M. T. Fukunaga, J. R. Guimaraes, R. Bertazzoli, *Chem. Engineering J.* 136 (2008) 236
3. M. H. Zhou, J. J. He, *Electrochimica Acta* 53 (2007) 1902
4. U. G. Akpan, B. H. Hameed, *J. Hazard. Mater.* 170 (2009) 520
5. D. Ravelli, D. Dondi, M. Fagnoni, A. Albini, *Chem. Soc. Rev.* 18 (2009) 1999
6. R. T. Pelegrini, R. S. Freire, N. Duran, et al., *Environ. Sci. Technol.* 35 (2001) 2849
7. Y. J. Feng, X. Y. Li, X. Li, et al, *Water Res.* 39 (2005) 1972
8. D. L. He, M. Sunil, *J. Electroanal. Chem.* 568 (2004) 19
9. C. Borrás, C. Berzoy, J. Mostany, J. C. Herrera, B. R. Scharifker, *Appl. Catal. B Environ.* 72 (2007) 98
10. S. Tanaka, Y. Nakata, T. K. Yustiawati, M. Kawasaki, H. Kuramitz, *J. Appl. Electrochem.* 32 (2002) 197
11. A.M. Polcaro, S. Palmas, F. Renoldi, M. Mascia, *J. Appl. Electrochem.* 29 (1999) 147
12. B. Correa-Lozano, C. Comninellis, A. D. Battisti, *J. Appl. Electrochem.* 27 (1997) 970
13. X. Chen, F. Gao, G. Chen, *J. Appl. Electrochem.* 35 (2005) 185
14. G. H. Zhao, X. Cui, M. C. Liu, et al., *Environ. Sci. Technol.* 43 (2009) 1480
15. P. Q. Li, G. H. Zhao, X. Cui, et al., *J. Phys. Chem. C* 113 (2009) 2375
16. G. H. Chen, X. M. Chen, P. L. Yue, *J. Phys. Chem. B* 106 (2002) 4364
17. R. Berenguera, C. Quijadab, E. Morallon, *Electrochimica Acta* 54 (2009) 5230
18. Y. H. Cui, Y. J. Feng, Z. Q. Liua. *Electrochimica Acta* 54 (2009) 4903
19. M. E. Makgae, C. C. Theron, W. J. Przybylowicz, A.M. Crouch, *Mater. Chem. Phys.* 2 (2005) 559
20. F. Vicent, E. Morallon, C. Quijada, J. L. Vazquez, A. Aldaz, *J. Appl. Electrochem.* 28 (1998) 607
21. L. X. Yang, S. L. Luo, Q. Y. Cai, S. Z. Yao, *Chinese Science Bulletin* 55 (2010) 331
22. A.Ghicov, P. Schmuki, *Chem. Commun.* 20 (2009) 2791
23. R. Sanju, C S. Roy, M. Paulose, et al., *Physical Chem. Chemical Phys.* 12 (2010) 2780
24. X. Cui, G. H. Zhao, Y. Z. Lei, H. X. Li, P. Q. Li, M. C. Liu., *Mater. Chem. Phys.* 113 (2009) 314
25. Y. Chen, L Hong, H. M. Xue, W. Q. Han, L. J. Wang, X. Y. Sun, J. S. Li, *J. Electroanal. Chem.* 648 (2010) 119
26. A.S. Huang, G. H. Zhao, H. X. Li., *Chinese Chemical Letters* 18 (2007) 997
27. K. Matsui, T. Kyotani, A. Tomita., *Advanced Materials* 14 (2002) 1216
28. H. Xu, Q. Zhang, C. L. Zheng, W. Yan, W. Chu, *Applied Surface Science*, 257 (2011) 8478
29. F. Montilla, N. E. Morallo, A. D. Battisti, A. Benedetti, H. Yamashita, J. L. Vazquez, *J. Phys. Chem. B.* 108 (2004) 5036
30. H. Y. Ding, Y. J. Feng, J. F. Liu, *Materials Letters* 61 (2007) 4920
31. X. M. Chen, G. H. Chen, *Electrochimica Acta* 50 (2005) 4155